Available online at www.sciencedirect.com
ScienceDirect
International Journal of Heat and Mass Transfer 51 (2008) 3913–3923
International Journal of HEAT and MASS TRANSFER
www.elsevier.com/locate/ijhmt

Estimation of thermal and mass diffusivity in a porous medium of complex structure using a lattice Boltzmann method

Namgyun Jeong [a], Do Hyung Choi [a,*], Ching-Long Lin [b]

[a] Department of Mechanical Engineering, Korea Advanced Institute of Science and Technology, Daejeon 305-701, Republic of Korea
[b] IIHR – Hydroscience and Engineering and Department of Mechanical and Industrial Engineering, The University of Iowa, Iowa City, IA 52242-1585, USA

Received 11 June 2007; received in revised form 15 November 2007
Available online 5 March 2008

Abstract

The thermal and mass diffusivity in a porous medium of complex structure is studied by using the lattice Boltzmann method. The media under consideration include two-dimensional medium with an array of periodically distributed circular and square cylinders, three-dimensional granular medium of overlapping or non-overlapping spherical and cubical inclusions of different size, and randomly generated fibrous medium. The calculated effective diffusivities are in good agreement with existing analytical and numerical results when the inclusions, regardless of their shapes, are not overlapped. For the medium of overlapping inclusions, the effective diffusivity deviates from existing correlations as the inclusion fraction increases. In particular, the deviation increases dramatically if the thermal diffusivity of the inclusion is greater than that of the fluid in the medium for enhanced thermal conduction. A new empirical correlation between the effective diffusivity and the volume fraction for the medium of overlapping inclusions is proposed.

Keywords: Lattice Boltzmann method; Porous medium; Granular/fibrous inclusions; Effective thermal/mass diffusivity

1. Introduction

The macroscopic effective transport properties of a porous medium, such as permeability and diffusivity, are of great practical importance in applications of heat exchangers, filtration systems, or any engineering device that utilizes a porous medium. It is because that the microscopic flow analysis in the pore region of a porous medium is neither computationally feasible nor cost-effective when only the macroscopic behavior of the transport phenomenon is of interest.

For permeability, Jeong et al. [1] carried out a series of calculations using the lattice Boltzmann method (LBM) and obtained the drag characteristics of the porous medium of various structures at different flow conditions. As for the subject of effective diffusivity and conductivity, it also has been treated by numerous researchers. Among theoretical approaches, Maxwell [2] calculated the effective electrical resistance of a compound medium consisting of scattered non-overlapping small spheres. Weissberg [3] estimated the upper bound of the effective diffusion coefficient in a porous medium in terms of simplified statistical parameters by considering idealized spheres whose centers are randomly placed. The results can be applied to randomly overlapped spheres of either uniform or non-uniform sizes. For the fibrous medium, Koch and Brady [4] developed a theory based on ensemble averages to determine the effective diffusivity. They also examined the effects of the Peclet number, $Pe = Ua/D_C$, where U is the average velocity through the bed, a is the fiber radius, and D_C is the molecular diffusivity of the solute in the fluid. Using the weighted geometric mean, Nield [5] proposed a formula for the effective thermal conductivity for a porous medium whose constituents have moderately different conductivities.

For numerical approaches, Monte Carlo simulations have been carried out to investigate the Knudsen diffusion

* Corresponding author. Tel.: +82 42 869 3018; fax: +82 42 869 3210.
E-mail address: d-h-choi@kaist.ac.kr (D.H. Choi).

0017-9310/$ - see front matter © 2008 Elsevier Ltd. All rights reserved.
doi:10.1016/j.ijheatmasstransfer.2007.11.045

Nomenclature

C	macroscopic mean concentration
c_Q	lattice dependent coefficient
D,D_{eff}	diffusivity, effective diffusivity
D_P	local molecular or thermal diffusivity
D_C,D_I	molecular or thermal diffusivity of the fluid and the solid
d	diameter of a fiber
e_α,$e_{\alpha i}$	discrete velocity, microscopic velocity
f_α, $\tilde{f}_\alpha$	pre- and post-collision state of the particle distribution function
f_α^{eq}	equilibrium particle distribution function
J_α,K_α	specially chosen constants for heat or mass-transfer simulation, Eq. (2)
L	side length of the calculation domain
u_i	macroscopic velocity

Greek symbols

ε	porosity
ϕ	solid volume fraction
τ	non-dimensional relaxation times
ξ	concentration of species or temperature

of gases and the effective diffusivities in the porous medium of various structures. Riley et al. [6] applied Monte Carlo simulations to obtain the effective diffusivities in porous media whose inclusions have different diffusivity from that of bulk phase. They considered two-dimensional (2D) rounded inclusions or three-dimensional (3D) spherical inclusions of uniform size and three types of structure: uniformly placed non-overlapping inclusion, inclusion clustered in groups of 50, and arbitrarily overlapping inclusion. Trinh et al. [7] determined the effective diffusion coefficients in a porous medium by using Monte Carlo simulations of point-like molecules in random and structured media. For the structured media, uniformly distributed inclusions of circular or square cylinders in 2D and spheres or cubes in 3D were considered with staggered, in-line and face-centered arrangements. All the inclusions were impermeable. Sahimi and Stauffer [8] used the lattice gas automata model to calculate the permeability and effective diffusivity of 2D stratified and heterogeneous porous media. Alvarez-Ramirez et al. [9] calculated the effective diffusivity of a 2D heterogeneous medium of irregular shape for various inclusion fractions using the LBM. Their results were in good agreement with Monte Carlo simulations of tracer diffusion as well as Maxwell's equation when the inclusion fraction is small.

The LBM is computationally more efficient than the direct simulation Monte Carlo method and the lattice gas automata model. Therefore it is adopted in the current study. The objectives of this research are twofold. The first objective is to examine thermal conductivity and mass diffusivity in both 2D and 3D porous media of various structures by using the LBM, and compare the results with existing analytical and numerical studies. The second objective aims to improve the empirical correlation between the effective diffusivity and the volume fraction for some porous media. The structure of the porous medium depends on the way how it is made, and on the type or purpose of experiment. For example, for solid oxide fuel cells (SOFC), some inclusions are overlapped, but some are non-overlapped. Thus, both overlapped and non-overlapped cases are considered here. The media under consideration include the granular medium made up of 2D circular and square cylinders, 3D spheres and cubes in staggered and in-line arrangements, and 3D fibrous media of cylindrical shape. Because the effective mass diffusivity and the effective thermal conductivity of a medium are governed by the equations of the same form, no distinction between them is made in estimation of these properties.

2. Numerical method

The discretized Boltzmann equation without an external forcing term reads

$$f_\alpha(\vec{x}+\vec{e}_\alpha\delta t, t+\delta t) - f_\alpha(\vec{x},t) = -\frac{1}{\tau}(f_\alpha - f_\alpha^{\text{eq}})|_{(\vec{x},t)} \tag{1}$$

where f_α is the particle distribution function, $e_{\alpha i}$ is the microscopic velocity, and τ is the non-dimensional relaxation time.

For thermal or mass transport, the equilibrium distribution function is expressed as [10]

$$f_\alpha^{\text{eq}} = \xi(J_\alpha + K_\alpha e_{\alpha i}\cdot u_i) \tag{2}$$

Here the concentration ξ is given by

$$\xi = \sum_\alpha f_\alpha \tag{3}$$

and J_α and K_α are constants, where J_α is determined from $\sum_\alpha f_\alpha^{\text{eq}} = \sum_\alpha f_\alpha$ and $K_\alpha = 1/2$.

Usually, the D2Q9 square lattice and the D3Q15 15-velocity LBM models shown in Fig. 1 are used for 2D and 3D simulations [11]. However, it has been known that, for the mass transport simulation, the lattice directions may be reduced from 9 to 5 and 15 to 7 for 2D and 3D cases, respectively, without degrading the accuracy [12].

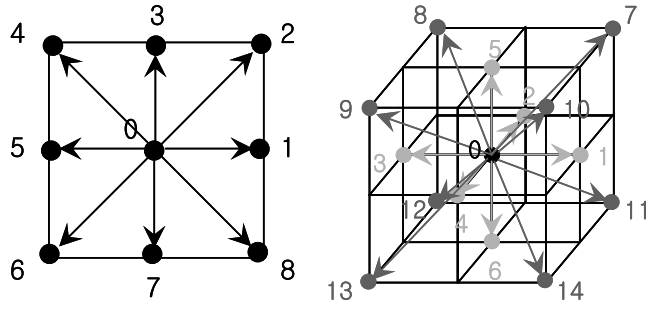

(a) D2Q9 model (b) D3Q15 model

Fig. 1. Schematic of the velocity directions for the D2Q9 and D3Q15 models: (a) D2Q9 model, (b) D3Q15 model.

For 2D cases, the discrete velocities become

$$e_{\alpha i} = \begin{cases} 0, & \alpha = 0 \\ (\pm 1, 0), (0, \pm 1), & \alpha = 1, 3, 5, 7 \end{cases} \tag{4}$$

and the value of J_α is

$$J_\alpha = \begin{cases} J_0, & \alpha = 0 \\ (1 - J_0)/4, & \alpha = 1, 3, 5, 7 \end{cases} \tag{5}$$

where J_0 is the rest fraction, which can be selected between 0 and 1.

For 3D cases, the discrete velocities $e_{\alpha i}$ and the value of J_α are given by

$$e_{\alpha i} = \begin{cases} 0, & \alpha = 0 \\ (\pm 1, 0, 0), (0, \pm 1, 0), (0, 0, \pm 1), & \alpha = 1, 2, \ldots, 6 \end{cases} \tag{6}$$

and

$$J_\alpha = \begin{cases} J_0, & \alpha = 0 \\ (1 - J_0)/6, & \alpha = 1, 2, \ldots, 6 \end{cases} \tag{7}$$

The diffusivity is then given by

$$D = c_Q (1 - J_0) \tau \frac{\delta x^2}{\delta t} \tag{8}$$

where c_Q is a lattice dependent coefficient, being equal to 1/2 and 1/3 for the 2D and 3D cases, respectively.

Eq. (1) may be recast into two computational steps:

$$\text{Collision step} : \tilde{f}_\alpha(\vec{x}, t) - f_\alpha(\vec{x}, t) = -\frac{1}{\tau}[f_\alpha(\vec{x}, t) - f_\alpha^{\text{eq}}(\vec{x}, t)] \tag{9}$$

$$\text{Streaming step} : f_\alpha(\vec{x} + \vec{e}_\alpha \delta t, t + \delta t) = \tilde{f}_\alpha(\vec{x}, t) \tag{10}$$

where f_α and $\tilde{f}_\alpha$ denote the pre- and post-collision states of the distribution function.

3. Validation test

To validate the procedure described in the previous section, a steady diffusion problem between two parallel walls, shown in Fig. 2a, is considered. The walls, located at $y = 0$ and 1, are kept at constant concentrations, ξ_L and $\xi_U (\xi_L < \xi_U)$, and a constant normal flow of velocity v_0 is injected through the lower wall and removed from the upper wall. The governing equation for the flow is

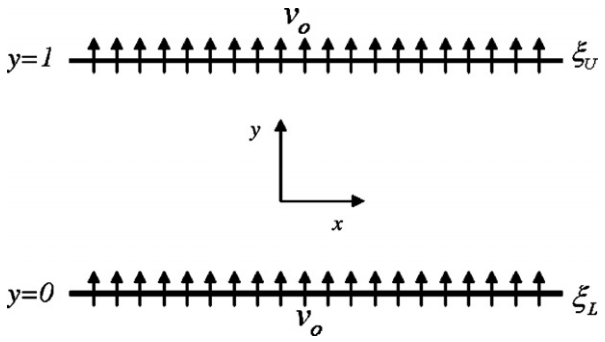

(a) Schematic of the problem

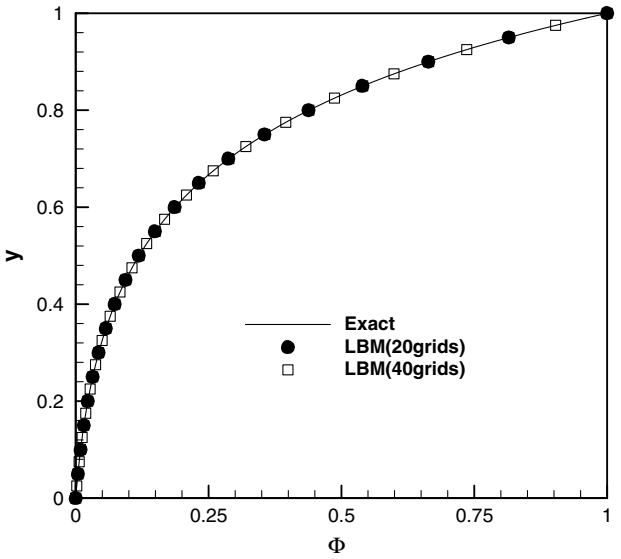

(b) Concentration profile

Fig. 2. Steady diffusion problem between parallel walls.

$$v_0 \frac{d\Phi}{dy} = D \frac{d^2\Phi}{dy^2} \tag{11}$$

where $\Phi = (\xi - \xi_L)/(\xi_U - \xi_L)$, and the solution Φ^* is given analytically by

$$\Phi^* = \frac{\exp(v_0 \cdot y/D) - 1}{\exp(v_0/D) - 1} \tag{12}$$

For $v_0/D = 4$, calculations are carried out with 20, 40, and 80 square grids between the two walls. The relaxation time τ and the rest fraction J_0 are fixed at 1 and 0.2, respectively, for all cases. The concentration profile, compared in Fig. 2b, shows an excellent agreement with the analytical solution and provides a degree of validation of the procedure. If we define the error as $E_n = \sum_n |\Phi - \Phi^*| / \sum_n |\Phi^*|$ with n being the number of grids, the error ratio ($= E_n/E_{2n}$) for two consecutive grids is calculated to be 3.795 for $n = 20$ and 3.893 for $n = 40$. The fact that the ratio

approaches to 4 as n increases confirms that the accuracy of the present scheme is of second-order.

4. Geometry, mesh size and boundary conditions

4.1. Granular media

The granular porous medium is constructed by uniformly distributed inclusions of circular or square cylinders in 2D, and by spheres or cubes in 3D for both staggered and in-line arrangements [1]. Taking advantage of geometric periodicity, it suffices to consider a single periodic module with the dimension of $L \times L$ ($L \times L \times L$) in 2D (3D).

For 2D media, we consider non-overlapping inclusions of uniform size. For 3D media, both overlapping and non-overlapping inclusions of uniform size and non-overlapping inclusions of non-uniform size are considered. Because the flow path in media with 3D overlapping non-uniformly sized inclusions can be closed even at large porosity for a certain case like in-line cube, it is not discussed here.

4.1.1. Non-overlapping uniform media

The domains of $L \times L$ and $L \times L \times L$ are divided into 200×200 lattices for 2D cases and $60 \times 60 \times 60$ lattices for 3D cases, respectively. It is appropriate to note here that these meshes, as well as those in the subsequent cases, have been chosen after the thorough mesh-dependency tests and were also used in the earlier hydrodynamic simulations [1]. In the current periodic setting for hydrodynamics, a prescribed concentration difference is imposed between the inlet and outlet boundaries. The unknown mass distribution functions at the inlet and outlet boundaries are denoted by f_1 and f_3, respectively. Like the implementation of a pressure difference in the hydrodynamic simulation [1,13], the two functions are assumed to differ by a constant

$$f_1|_{\text{in}} = f_1|_{\text{out}} + C, \tag{13}$$

$$f_3|_{\text{out}} = f_3|_{\text{in}} - C, \tag{14}$$

where the constant C is calculated from the concentration difference $\Delta\xi$ as

$$C = \frac{1}{2}[\Delta\xi - (f_0|_{\text{in}} - f_0|_{\text{out}} + f_5|_{\text{in}} - f_5|_{\text{out}} + f_4|_{\text{in}} - f_4|_{\text{out}} + f_6|_{\text{in}} - f_6|_{\text{out}} + f_2|_{\text{in}} - f_2|_{\text{out}})] \tag{15}$$

For the boundary condition on a solid wall at the mesoscopic level, the second-order halfway-bounceback scheme [1] is adopted. For this scheme the solid wall is placed in the middle between the lattice nodes. The boundary conditions described above are similar to those in Yoshino and Inamuro [14] except that the lattice nodes in their calculations are placed on the boundary. They considered only the non-permeable inclusions. The present halfway-bounce-

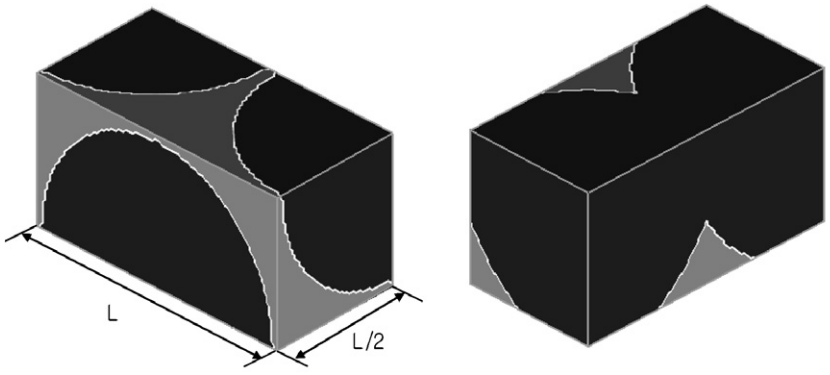

(a) Overlapping uniform spheres

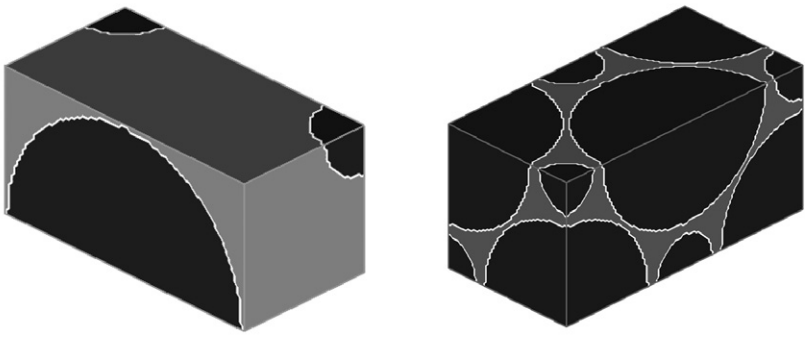

(b) Non-overlapping non-uniform spheres

Fig. 3. Calculation domain for the granular porous media: (a) overlapping uniform spheres, (b) non-overlapping non-uniform spheres.

back scheme is better suited for treating the permeable or conductive inclusions.

4.1.2. Overlapping uniform media

When the inclusions are overlapped, the flow passage is narrower than that of the non-overlapping media. More lattices are needed to achieve comparable accuracy, and 100 lattices are used in each direction. To reduce the computation time further, the domain is halved for the cases of sphere as shown in Fig. 3a, by taking full advantage of symmetry. The inlet and outlet boundary conditions are the same as those described in 4.1.1, and the symmetric boundary condition is imposed at other boundary faces [15].

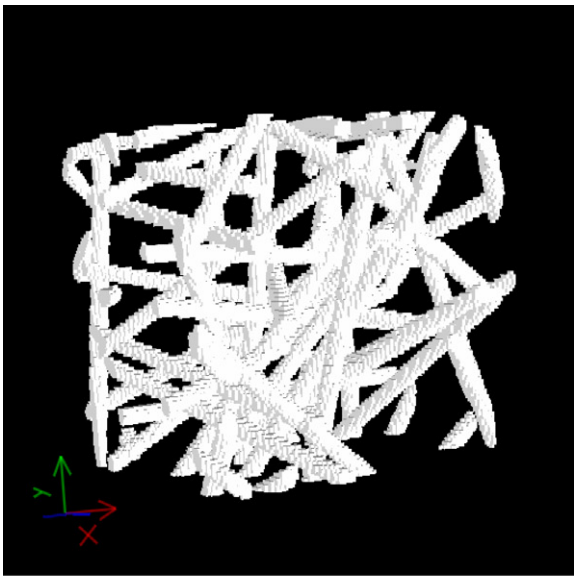

(a) $\phi = 0.01857$ with $d = 5$

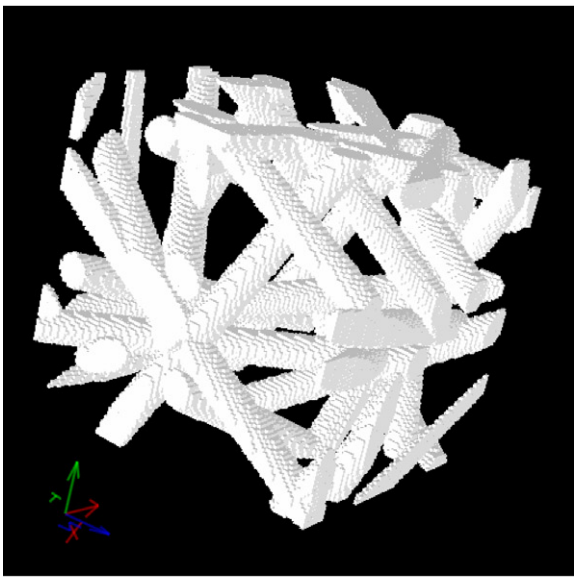

(b) $\phi = 0.1789$ with $d = 10$

Fig. 4. The micro-structure of fibrous porous media: (a) $\phi = 0.01857$ with $d = 5$, (b) $\phi = 0.1789$ with $d = 10$.

4.1.3. Non-overlapping non-uniform media

For non-uniform media, inclusions of two different sizes are placed alternately in each direction for the in-line arrangement while, for the staggered arrangement, the larger inclusion is placed at the center of the smaller eight (or four if 2D) and vice versa. Fig. 3b shows the typical calculation domains for spheres in both arrangements. $122 \times 61 \times 61$ and $86 \times 43 \times 43$ cubic lattices are used for the in-line and staggered cases, respectively. The ratio of the characteristic length of the inclusions is varied to be 1.5, 2.0, and 3.0. The boundary conditions are the same as those for the overlapping uniform medium in 4.1.2.

4.2. Fibrous media

An important feature of fibrous porous media is that the solid fraction is often much lower than that of a granular material because much less material is needed to form a structure. The fiber volume fraction ϕ, which equals $1 - \varepsilon$ with ε being the porosity of the medium, can easily be as low as 0.01 even in the real structures. In this study, ϕ ranges from 0.01857 to 0.4500 with the randomly oriented and overlapped fibers of cylindrical shape as shown in Fig. 4. For $\phi < 0.09$, the diameter of a fiber $d = 5$ is used, and for $\phi > 0.09$, $d = 10$. The domain is fitted by $100 \times 100 \times 100$ cubic lattices.

Unlike the granular cases, the fibrous porous structures are not periodic. Therefore, for the mass transport simulations, the equilibrium distribution functions with constant concentrations are imposed at the inlet and outlet boundaries as before, and the symmetry conditions at other boundaries.

5. Results and discussion

For the estimation of the effective diffusivity of a heterogeneous medium, the method of Alvarez-Ramirez et al. [9] described below is adopted. Consider a heterogeneous medium with either permeable or non-permeable inclusions imposed with a concentration gradient as shown in Fig. 5. The mass transport can be locally described by the diffusion equation

$$\frac{\partial \xi}{\partial t} - \nabla(D_P \nabla \xi) = 0 \tag{16}$$

where ξ is the molar concentration, and D_P is the local molecular diffusivity which is equal to D_C in the continuous phase and D_I in the inclusion phase. The pore size is generally much smaller than the typical length scale and the mass transport in the domain may be described by the macroscopic diffusion equation

$$\frac{\partial C}{\partial t} - D_{\text{eff}} \nabla^2 C = 0 \tag{17}$$

where C is the macroscopic mean concentration, and D_{eff} is the effective diffusivity in the X_1 direction. The effective diffusivity may be defined as follows:

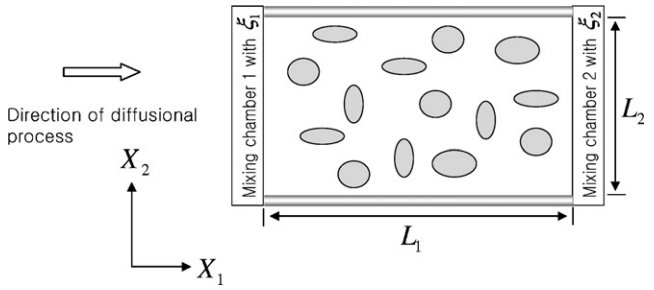

Fig. 5. Experimental setup for the estimation of effective diffusivity.

$$D_{\text{eff}} = \frac{w^*}{w} D_C \tag{18}$$

where

$$w = D_C(\xi_2 - \xi_1)L_2/L_1$$
$$w^* = \int_0^{L_2} D_P(\partial\xi/\partial X_1)_{X_1=L_1} \mathrm{d}X_2 \tag{19}$$

The steady-state concentration distribution $\xi(X_1, X_2)$, which is needed to estimate w^*, is obtained by solving the Eq. (16) for the steady state. It is noteworthy that, although the LBM described in the previous section is for general cases, the problems considered in the present study are for pure diffusion and no velocity field is imposed as is noted in Eq. (16).

5.1. 2D diffusion

Alvarez-Ramirez et al. [9] used 500×500 grid nodes, and the distribution of phase nodes was made randomly or deterministically. Their 2D results show good agreement with those of Monte Carlo simulations of tracer diffusion. They also compared their results with the following equation based on Maxwell [2]

$$\frac{D_{\text{eff}}}{D_C} = \frac{2D_C + D_I - 2\phi(D_C - D_I)}{2D_C + D_I + \phi(D_C - D_I)} \tag{20}$$

In 2D simulations, the effective diffusivities for porous structures consisting of either permeable or non-permeable inclusions are estimated, and compared with earlier results. Calculations are carried out for flows across a bank of circular cylinders in staggered or in-line arrangement. The domain is divided into 200×200 lattices. Fig. 6a shows the effective diffusivities for permeable inclusions. For two values of D_C/D_I considered, namely 2.0 and 4.0, the results agree well with those of Alvarez-Ramirez et al. [9] even though the inclusions are not distributed in the same manner. These two, however, agree less favorably with Maxwell's equation. The discrepancy increases with increasing D_C/D_I. It is interesting to note that the results are independent of the porous medium structure.

The results for non-permeable inclusions in Fig. 6b are in very good agreement with the Monte Carlo simulation of Trinh et al. [7] for all cases considered. Unlike in the cases of permeable inclusion, they are in less agreement

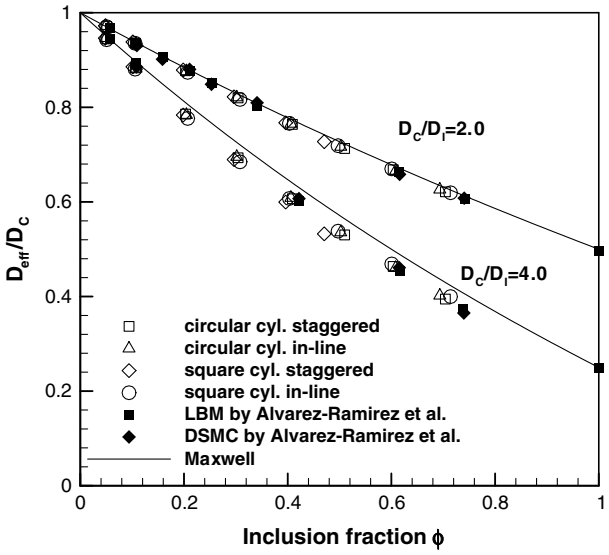

(a) Permeable inclusions.

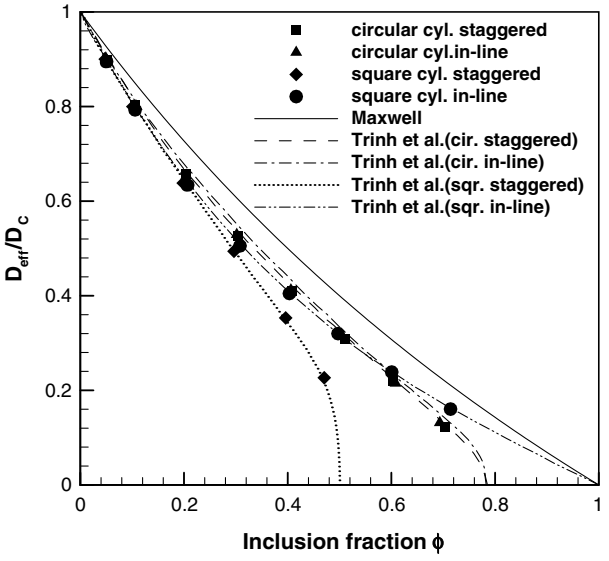

(b) Non-permeable inclusions.

Fig. 6. Effective diffusivity for 2D inclusions.

with Maxwell's equation. The results for various cases are seen to coalesce when the inclusion fraction ϕ is small. However, they start to deviate from one another as ϕ increases. The case for the staggered square cylinders deviates from the other curves early since the flow passage is blocked rapidly when ϕ becomes close to 0.5.

The concentration fields for various cases are presented in Fig. 7. The inclusion fractions for these cases are close to one another: 0.4091, 0.4062 for staggered and in-line circular cylinders, and 0.3961, 0.4032 for staggered and in-line square cylinders, respectively. The equally spaced contours exhibit that the concentration varies rapidly as the flow passage becomes narrow. This attributes to the fact that the effective diffusivity of the staggered square cylinder case

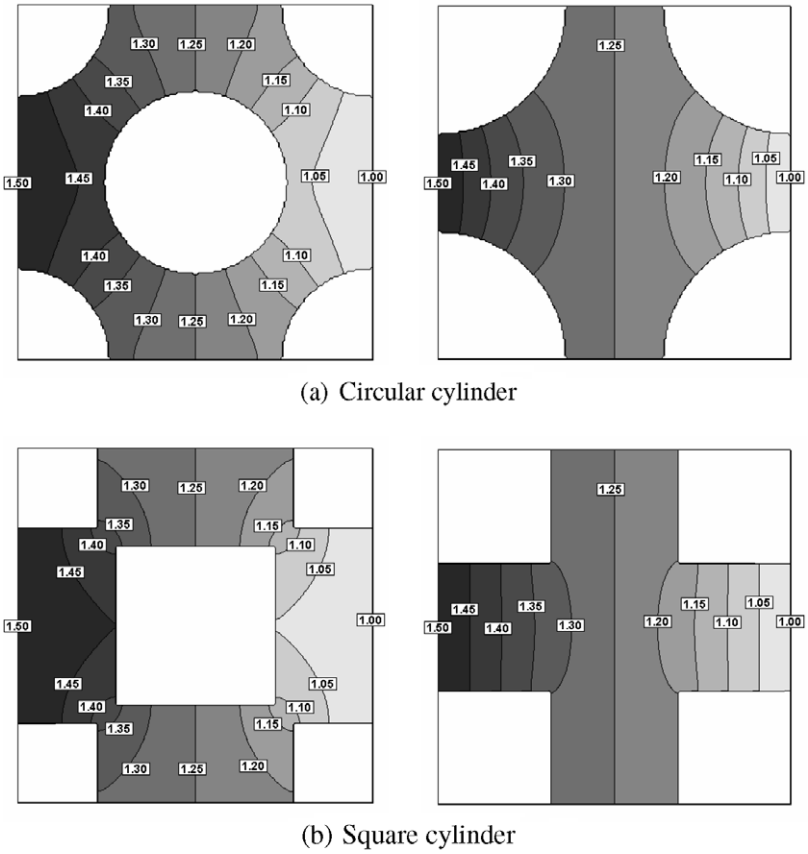

Fig. 7. Concentration distributions for 2D cases: (a) circular cylinder, (b) square cylinder.

deviates sharply from the rest as ϕ increases as is seen in Fig. 6b.

5.2. 3D diffusion – granular media

The effective diffusivities for 3D cases are estimated with various inclusion fractions in this section. In thermal heat-transfer problems, the thermal diffusivity (or conductivity) of the inclusion phase is usually larger than that of the continuous phase, and D_C/D_I becomes smaller than 1. Therefore 0.5, 0.25 and 0.1 are also considered in the 3D simulation. As the volume fraction increases, the effective diffusivity will decrease (increase) if D_C/D_I is larger (smaller) than 1.

5.2.1. Uniform non-overlapping granular media

The results for uniform non-overlapping granular media are shown in Fig. 8. The correlations of Maxwell (20) and Nield [5], obtained by using the weighted geometric mean

$$D_{\text{eff}} = D_C^{1-\phi} D_I^{\phi} \tag{21}$$

are included in the figure for comparison. When the difference between D_C and D_I is small irrespective of their ratio being greater or smaller than 1, the present results agree quite well with Maxwell's equation. From these results, one may conclude that Maxwell's equation can be used to estimate the effective diffusivity almost exactly not only for the spherical inclusions, but also for the cubic inclusions. As D_I becomes much larger than D_C, Maxwell's equation is found to underestimate the effective diffusivity, especially for the staggered cube case. Nield's equation seems to fare slightly better. For $D_C/D_I = 0.1$, the effective diffusivity is seen to vary from case to case. In other words, the diffusivity depends considerably on the inclusion shape and/or arrangement.

The effective diffusivities for non-permeable inclusions ($D_C/D_I = \infty$) are also seen to be in good agreement with Maxwell's equation when the inclusion fraction is less than 0.4. However, the agreement deteriorates as the inclusion fraction increases.

5.2.2. Uniform overlapping granular media

Fig. 9 presents the results for uniform overlapping granular media; solid and open symbols indicate non-overlapping and overlapping media, respectively. For $D_C/D_I = 2.0$ and 0.5, the results of various cases agree quite well with Maxwell's formula. However, increasing discrepancy is observed for $D_C/D_I = 4.0$ and 0.25 as ϕ increases except for the case of non-overlapping in-line cube. For $D_C/D_I = 0.1$ and when the inclusions are overlapped, the effective diffusivity is, in general, much higher than that of the non-overlapping cases, and neither Maxwell's nor Nield's correlation seems satisfactory. This is because the heat transfer is enhanced by the connected inclusions that

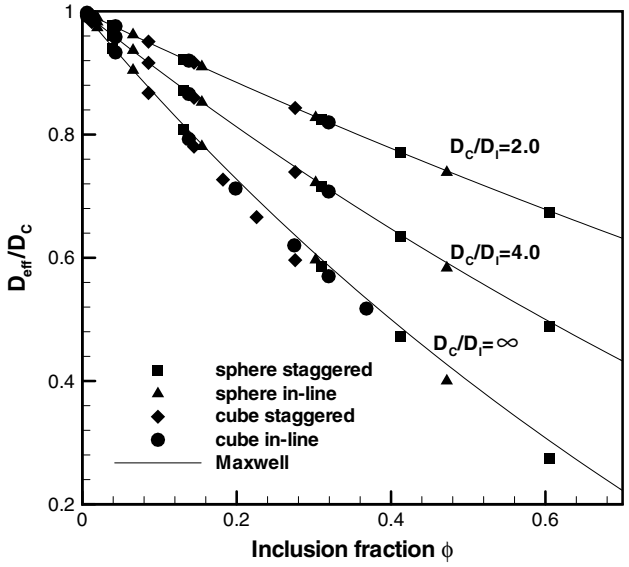

(a) $D_C/D_I > 1$

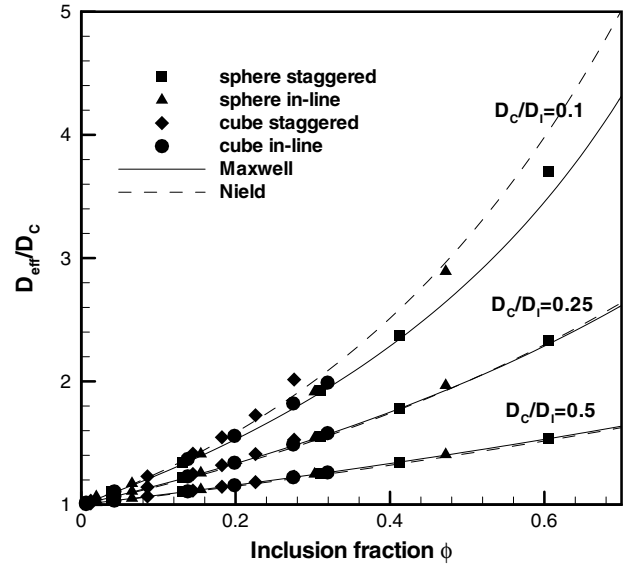

(b) $D_C/D_I < 1$

Fig. 8. Effective diffusivity for 3D inclusions (uniform non-overlapping granular media): (a) $D_C/D_I > 1$, (b) $D_C/D_I < 1$.

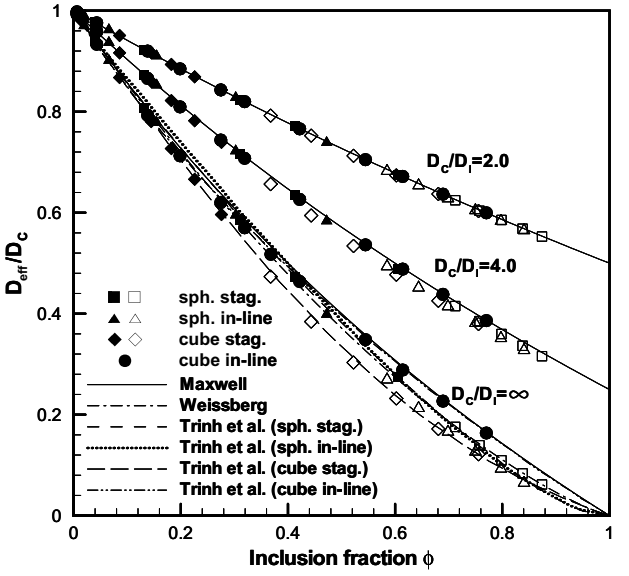

(a) $D_C/D_I > 1$

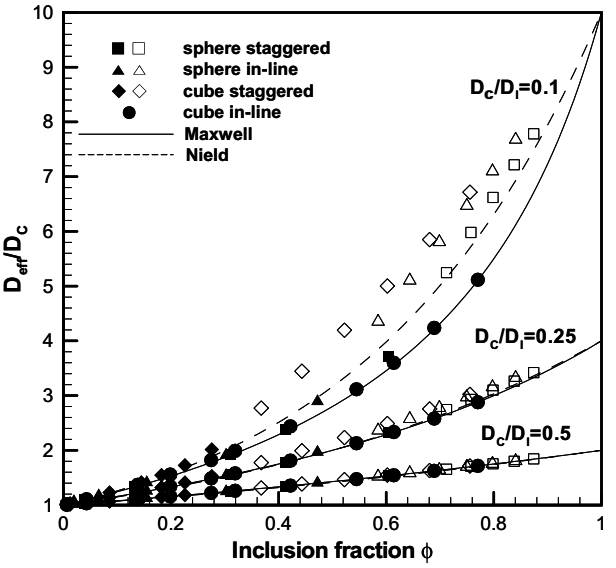

(b) $D_C/D_I < 1$

Fig. 9. Effective diffusivity for 3D inclusions (uniform overlapping granular media): (a) $D_C/D_I > 1$, (b) $D_C/D_I < 1$.

make the solid region larger. As there is no overlapped solid region before ϕ becomes 1 (all solid) for the in-line cube, it gives the lowest diffusivity and follows Maxwell's equation well.

The upper bounds for the effective diffusivity proposed by Weissberg [3], obtained by considering the statistical properties of the bed of spheres, are also presented

$$\frac{D_{\text{eff}}}{D_C} < \frac{1-\phi}{q} \tag{22}$$

where

$$q = 1 - \frac{1}{2}\ln(1-\phi) \tag{23}$$

when the spheres are randomly distributed.

For non-permeable inclusions, all results are seen to be in good agreement with those of Trinh et al. [7]. The results for the sphere are in good agreement with those of Weissberg [3], especially for the staggered arrangement whereas Maxwell's equation predicts higher values for the overlapping inclusions that have large ϕ. For the cube, the equation of Weissberg [3] does not fit the results well for either the staggered or the in-line case. However, the results for the in-line arrangement (non-overlapping inclusions) are in good agreement with Maxwell's equation. The Maxwell's equation appears well suited to estimate the effective diffusivity of the non-overlapping 3D granular media having inclusions of the same size.

5.2.3. Non-uniform non-overlapping granular media

Non-uniform inclusions, characteristic length ratios of 1.5, 2.0 and 3.0, are considered. The effective diffusivities for various cases are shown in Fig. 10. For permeable inclusions, it is seen from the figure that the inclusion arrangement and the shape or the size of the inclusions do not affect the effective diffusivity unless the difference between D_C and D_I is large. All results are in good agreement with Maxwell's equation except for the case of $D_C/D_I = 0.1$. As in the uniform non-overlapping granular medium, Nield's formula is seen to give a little better result than Maxwell's equation for cubical inclusions.

For non-permeable inclusions, the results for the cases of sphere lie closely together between the equations of Maxwell [2] and Weissberg [3]. The effects of the inclusion arrangement and the size ratio of the inclusions on the effective diffusivity do not seem significant. However, for the cases of cube, those effects become significant. For the in-line cube, the flow passage is closed if the inclusion fractions are about 0.6481, 0.5625 and 0.5185 when the size ratios of the inclusions are 1.5, 2.0, and 3.0, respectively. The discrepancy between the present results and the theoretical equations [2,3] becomes evident as the ratio of size increases. In contrast to the case of in-line cube, the agreement with the theoretical results does not deteriorate as the size ratio of the inclusions becomes large for the staggered arrangement.

5.3. 3D diffusion – fibrous media

Koch and Brady [4] presented the equations for the effective diffusivity of the fibrous media. However, they

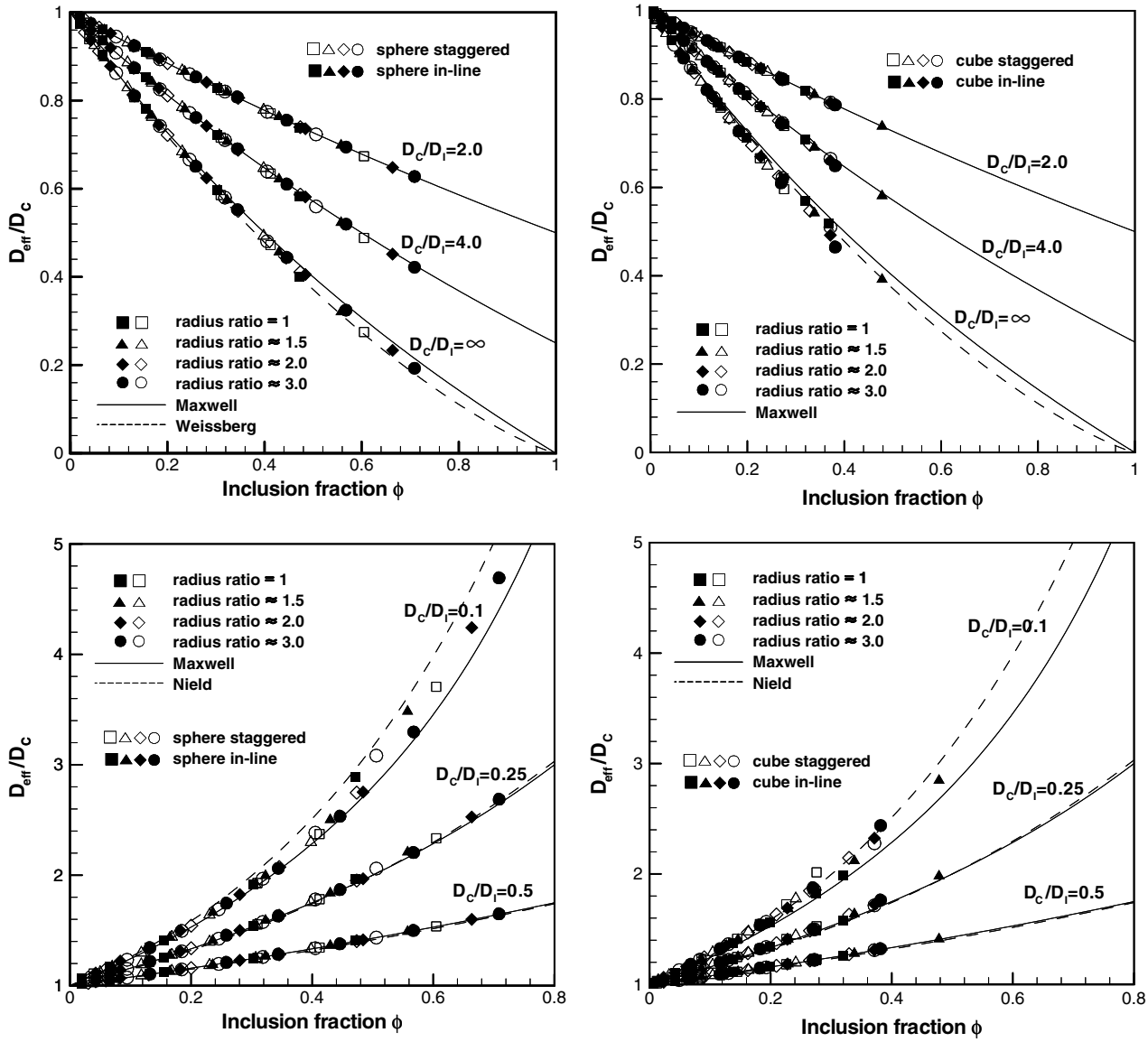

(a) Sphere (b) Cube

Fig. 10. Effective diffusivity for 3D inclusions (non-uniform non-overlapping granular media).

presented only the asymptotic behavior in the low volume fraction limit. For pure diffusion, if the fibers are impermeable, the effective diffusivity is given as follows:

$$\frac{D_{\text{eff}}}{D_C} = \frac{1}{1-\phi} - \frac{5}{3}\phi \tag{24}$$

This gives the effective diffusivity of infinite value when $\phi = 1$, and the minimum value, 0.9153 when $\phi = 0.2254$. Obviously, it is not suitable for the fibrous media whose volume fraction is large, and one may have to resort to other correlations or numerical simulation.

The volume fractions of the fiber considered in the present study are 0.01857, 0.07301 for $\phi < 0.09$, and 0.1789, 0.2739, 0.3609, and 0.4500 for $\phi > 0.09$. Fig. 11 shows

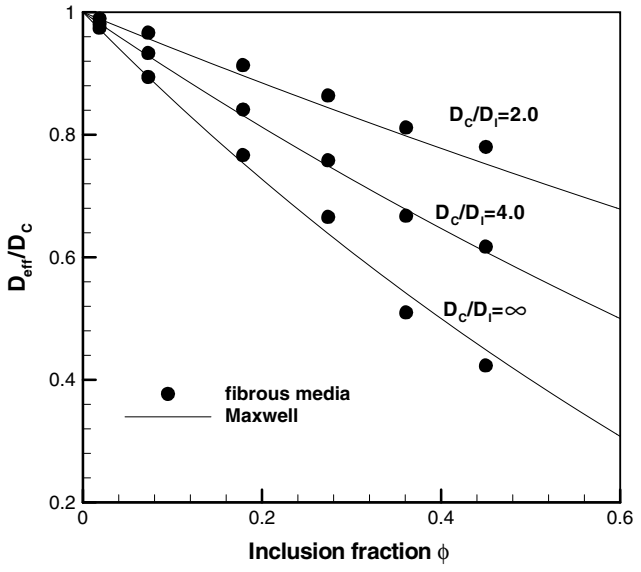

(a) $D_C/D_I > 1$

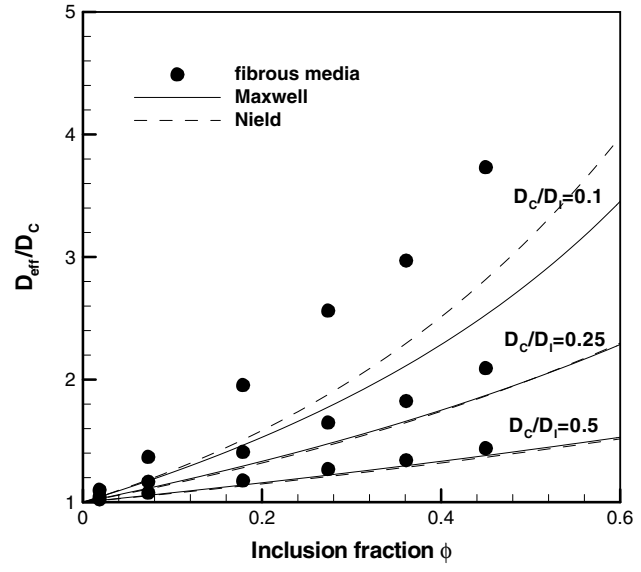

(b) $D_C/D_I < 1$

Fig. 11. Effective diffusivity for 3D fibrous media.

the effective diffusivities for these fibrous media. When $D_C/D_I > 1$ up to ∞ (non-permeable), the present results are relatively in good agreement with Maxwell's equation including the non-permeable case. The overall tendency is similar to that of granular media. When $D_C/D_I < 1$, however, the tendency is different from the granular cases: the discrepancy between the present results and existing correlations becomes fairly large as D_C/D_I decreases even when the volume fraction of inclusion is very small. It is because, for the fibrous medium, a long fiber that may extend from one end of the domain to the other enhances the conductive heat transfer even though the volume fraction is small.

By using a quadratic polynomial to present an empirical correlation for the effective diffusivity of the medium of overlapping inclusions, we have

$$\frac{D_{\text{eff}}}{D_C} = C_0 + C_1\phi + C_2\phi^2 \tag{25}$$

From the condition that $D_{\text{eff}}/D_C = 1$ and D_I/D_C for $\phi = 0$ and 1, respectively, we obtain $C_0 = 1$ and $C_1 + C_2 = D_I/D_C - 1$. Fitting the data of Fig. 11b in a least-squares sense, C_1 and C_2 are finally determined as

$$C_1 = -0.285 + 0.664\frac{D_I}{D_C} - 0.0265\left(\frac{D_I}{D_C}\right)^2 \tag{26}$$

$$C_2 = -0.715 + 0.336\frac{D_I}{D_C} + 0.0265\left(\frac{D_I}{D_C}\right)^2 \tag{27}$$

In Fig. 12, the above correlation is compared with the results for overlapping granular medium and fibrous medium. The correlation is in good agreement with the data of fibrous medium, and the data of overlapping granular medium are located between the correlation and Nield's equation.

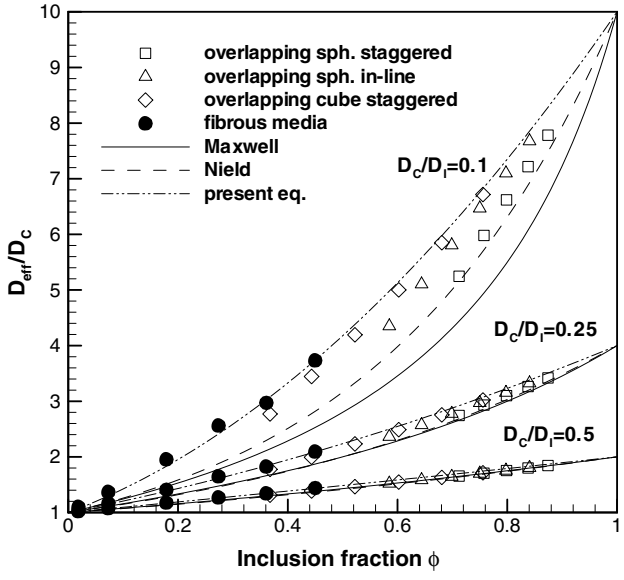

Fig. 12. Comparison among the present correlation, Maxwell's and Nield's equations, and the data of 3D fibrous and overlapping granular media.

6. Conclusions

The effective diffusivity through the porous medium is successfully estimated by the lattice Boltzmann method. The results that have been obtained for various 2D and 3D structures are compared with those of other numerical simulations and/or analytic equations. The results, generally, are in good agreement with the existing numerical results. The analytic equation of Maxwell is suitable for non-overlapping medium or for permeable inclusions whose diffusivity is not much different from that of the fluid. When the diffusivity through the inclusion is much larger than that of the fluid, the effect of the inclusion shape or arrangement becomes significant and the results deviate rather sharply from Maxwell's or Nield's prediction as the inclusion fraction increases. For 3D non-permeable inclusions with moderate inclusion fraction, the analytical solution of Maxwell is adequate in estimating the effective diffusivity well even for the fibrous material.

Acknowledgement

This work was supported by the Ministry of Commerce, Industry, and Energy through the project, "Development of 5 kW_e Cogeneration SOFC System".

References

[1] N. Jeong, D.H. Choi, C.L. Lin, Prediction of Darcy–Forchheimer drag for micro porous structures of complex geometry using the lattice Boltzmann method, J. Micromech. Microeng. 16 (2006) 2240–2250.

[2] J.C. Maxwell, A Treatise on Electricity and Magnetism, third ed., vol. 1, Dover, New York, 1954.

[3] H.L. Weissberg, Effective diffusion coefficient in porous media, J. Appl. Phys. 34 (9) (1963) 2636–2639.

[4] D.L. Koch, J.F. Brady, The effective diffusivity of fibrous media, AIChE J. 32 (4) (1986) 575–591.

[5] D.A. Nield, Estimation of the stagnant thermal conductivity of saturated porous media, Int. J. Heat Mass Transfer 34 (1991) 1575–1576.

[6] R.M. Riley, F.J. Muzzio, H. Buettner, S.C. Reyes, Diffusion in heterogeneous media: application to immobilized cell systems, AIChE J. 41 (1995) 691–700.

[7] S. Trinh, P. Arce, B.R. Locke, Effective diffusivities of pin-like molecules in isotropic porous media by Monte Carlo simulation, Transport in Porous Media 38 (2000) 241–259.

[8] M. Sahimi, D. Stauffer, Efficient simulation of flow and transport in porous media, Chem. Eng. Sci. 9 (1991) 2225–2233.

[9] J. Alvarez-Ramirez, S. Nieves-Mendoza, J. Gonzalez-Trejo, Calculation of the effective diffusivity of heterogeneous media using the lattice-Boltzmann method, Phys. Rev. E 53 (3) (1996) 2298–2303.

[10] S.P. Sullivan, F.M. Sani, M.L. Johns, L.F. Gladden, Simulation of packed bed reactors using lattice Boltzmann methods, Chem. Eng. Sci. 60 (2005) 3405–3418.

[11] Y. Qian, D. d'Humières, P. Lallemand, Lattice BGK models for the Navier–Stokes equation, Europhys. Lett. 17 (1992) 479–484.

[12] T. Zeiser, P. Lammers, E. Klemm, Y.W. Li, J. Bernsdorf, G. Brenner, CFD-calculation of flow dispersion and reaction in a catalyst filled tube by the lattice Boltzmann method, Chem. Eng. Sci. 56 (2001) 1697–1704.

[13] T. Inamuro, M. Yoshino, F. Ogino, Lattice Boltzmann simulation of flows in a three-dimensional porous structure, Int. J. Numer. Meth. Fluids 29 (1999) 737–748.

[14] M. Yoshino, T. Inamuro, Lattice Boltzmann simulation for flow and heat/mass transfer problems in a three-dimensional porous structure, Int. J. Numer. Meth. Fluids 43 (2003) 183–198.

[15] R. Mei, W. Shyy, On the finite difference-based lattice Boltzmann method in curvilinear coordinates, J. Comp. Phys. 143 (1998) 426–448.